Thermomechanical fatigue – Mechanism-based considerations on the challenge of life assessment

Hans-Jürgen Christ[1,*]

[1]Institut für Werkstofftechnik, Universität Siegen, Paul-Bonatz-Str. 9-11, D-57076 Siegen, Germany

Abstract. The combination of cyclic mechanical and cyclic thermal loading leads to thermomechanical fatigue (TMF) which is considered to be the primary life-limiting factor for engineering components in many high-temperature applications. Extensive low-cycle fatigue (LCF) data, which is traditionally used for design purposes, has been generated isothermally on various high-temperature materials, and thus, it is tempting to try to predict TMF life based mainly on isothermal LCF data. In this contribution, studies on different metallic structural high-temperature materials, which have mainly been carried out in the author's laboratory, are reviewed addressing the question, in which way and to which extent a reliable, unerring and robust TMF life assessment is possible on the basis of isothermally obtained fatigue life data. It is shown by means of examples that a sound TMF life prediction first of all requires a detailed mechanistic understanding of the isothermal cyclic stress-strain response and the relevant damage mechanisms. Furthermore, the TMF-specific peculiarities in both the non-isothermal cyclic stress-strain behaviour and the non-isothermal damage evolution process must be known. If all these requirements are fulfilled and reflected in the TMF life assessment methodology applied, a reasonable predictive accuracy can be attained.

1 Introduction

Thermomechanical fatigue (TMF) is the primary life-limiting factor for engineering components in many high-temperature applications. For example, during the transient regimes of start-up and shut-down operations, blades in gas turbines are submitted to low-cycle TMF due to the temperature gradients generated caused by temperature variations often in combination with internal air cooling (see Fig. 1). Depending on the location of the volume element considered and the cooling situation, various types of strain-temperature phasing can arise. In laboratory testing most commonly the two extreme cases, in-phase (IP) and out-of-phase (OP) TMF, are studied.

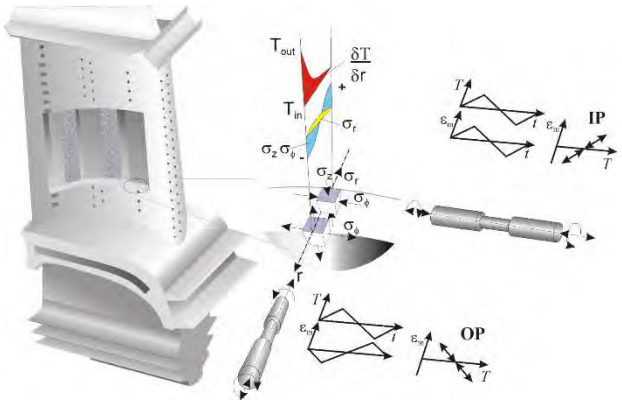

Fig. 1. Origin and sites of thermomechanical fatigue loading in cooled turbine blades.

Due to the life-reducing effect of TMF it is important to investigate the TMF behaviour of engineering materials in order to model thermomechanical fatigue life correctly. On the other hand, for many structural materials extensive, isothermally determined low-cycle fatigue (LCF) data has been generated at various temperatures, and thus, it would be very efficient, if TMF life could be predicted based largely on isothermal LCF data. However, it is well known that depending on the actual loading conditions damage can evolve differently [1,2], and life prediction may well be non-conservative if the relevant damage mechanisms are not captured accurately. Still, studies that assess the predictive capabilities of TMF life models [1-10] are rare. Part of this results from the large number of model parameters that need to be determined for the more advanced life models. Given this scenario, the objective of the present study is to answer the question, whether TMF life can in principle be considered to be predictable from isothermally obtained data. Furthermore, the requirements with respect to material behaviour and knowledge base are considered which have to be fulfilled to allow for the development of TMF life models that are robust, easily implemented, and do not require sophisticated testing.

This paper is based on the results which have been obtained in various studies on the TMF behaviour of structural metallic materials in the author`s laboratory during more than two decades. Selected results are presented in order to illustrate exemplarily the broad spectrum of phenomena. After showing the strong effect of temperature on the isothermal cyclic stress-strain behaviour and the damage mechanisms, some peculiarities resulting from the varying temperature of TMF are illustrated. Then it is documented that TMF life prediction is very difficult, if cyclic plasticity is low.

* Corresponding author: hans-juergen.christ@uni-siegen.de

Brittle behaviour often means that the stage of fatigue crack initiation dominates fatigue life. Then the contribution of the stage of crack propagation is less important leading to an almost unpredictable behaviour. Finally, the need of a close correlation of the relevant damage mechanism and the suitable damage parameter is verified.

2 Materials and particular experimental details

This study reports on the behaviour of four different materials which were investigated in the framework of Ph.D. works [11-15]. An AISI 304 L-type stainless steel was used, as a large amount of data generated on this material in isothermal LCF tests, creep-fatigue tests and TMF tests are available.

The second material chosen was X8019+12.5SiC$_P$ that is a dispersion-strengthened SiC particulate-reinforced aluminium alloy (matrix composition: Al-8Fe-4Ce, in wt.%). Within the matrix, fine and thermally very stable dispersoids with a high volume fraction of 0.23 are present. The dispersoids provide for excellent creep properties at elevated temperatures. The reinforcement with 12.5 vol.% SiC particulates increases both the elastic modulus and the fatigue crack growth threshold of the alloy.

As the third material the high-temperature titanium alloy IMI 834 was applied which is a near-α Ti alloy of nominal composition Ti-5.8Al-4.0Sn-3.5Zr-0.7Nb-0.5Mo-0.35Si-0.06C (in wt.%). All data used in this study was obtained on the bimodal microstructure which is designed to yield an optimum compromise between creep and fatigue performance.

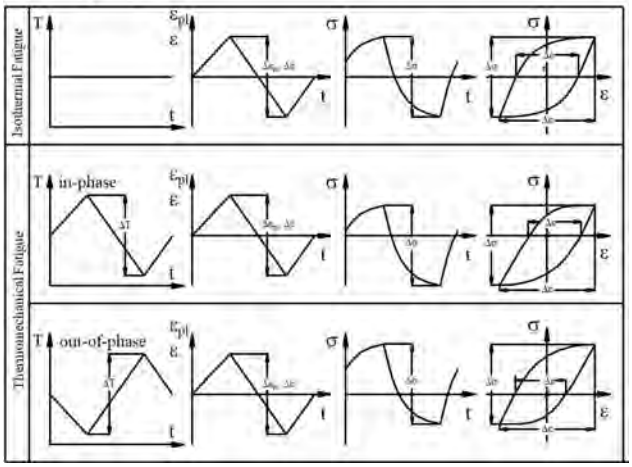

Fig. 2. Types of laboratory tests used in this study.

Different third generation near-γ TiAl alloys were also used in this study. The alloy γ-PX (similar to TNB-V5) was produced by Plansee AG, Austria with a nominal composition of Ti-47Al-5.1Nb-0.25C-0.4B (at.%). The material was subjected to a heat treatment such that a duplex microstructure was attained. The γ-alloy Ti-45Al-8Nb-0.2C (at.%), referred to as TNB-V2, has been developed by *Helmholtz Zentrum Geesthacht*. The heat treatment applied resulted in a nearly lamellar microstructure.

The Ductile to Brittle Transition Temperature (DBTT), which is a significant quantity for TiAl alloys, was determined for the alloys considered to be about 750°C. The transition from brittle to ductile behaviour manifests itself in a strong increase in fracture ductility when exceeding the temperature of 750°C because of the onset of dislocation climb.

In all cases, the isothermal fatigue (IF) and TMF tests evaluated (see Fig. 2) were selected such that a wide range of test parameters were covered. The TMF tests were of in-phase and out-of-phase type, *i.e.* maximum test temperature coincided with maximum strain (in tension) or minimum strain (in compression), respectively. All tests except of those on the γ-TiAl alloy were conducted in true-plastic-strain control, and a triangular wave form was used for the command signal. Because of the brittleness of the TiAl alloy, total-strain control had to be applied in this case

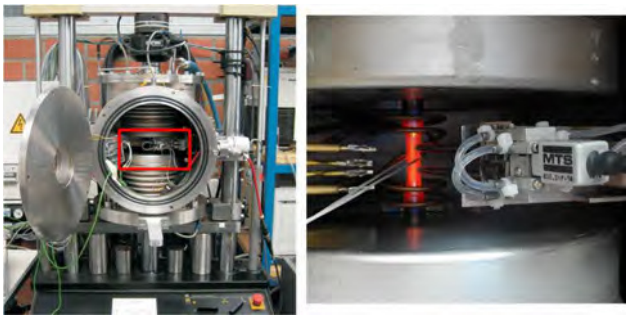

Fig. 3. Testing system used for high-temperature fatigue testing (left). View into the vacuum chamber (right) showing the induction coil, a ribbon-type thermocouple and a water-cooled extensometer.

A servohydaulic test system of type MTS 810 was applied for both the isothermal and thermomechanical fatigue tests. As can be seen in Fig. 3, this system is equipped with a vacuum chamber enabling tests in vacuum at a pressure below 10^{-5} mbar. These vacuum tests were carried out as reference tests in addition to the standard tests in air, in order to separate the environmental effect on fatigue life. The influence of environment can be very strong as depicted in Fig. 4 representing the ratio of the number of cycles until failure N_f in vacuum to N_f in air versus the mean temperature of OP tests at different total strain amplitudes Δε/2 carried out on TiAl-based alloys. It is clearly seen that this ratio increases strongly with increasing mean temperature reaching values of up to 60.

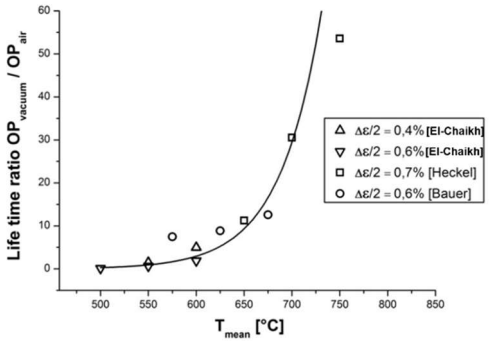

Fig. 4. Representation of the effect of environment (air or vacuum) on the TMF life for OP tests on TiAl-based alloys.

3 Results and discussion

3.1. Isothermal fatigue mechanisms

It is well-known and has been studied in detail that the cyclic deformation mechanism depends strongly on temperature applied in IF. Figure 5 tries to summarize some of these effects. While at low temperature dislocations motion is dominated by gliding, dislocation climb gains importance with increasing temperature. Most of the metallic materials show a strong interaction of point defects with moving dislocations giving rise to dynamic strain aging (DSA). The cyclic deformation response of a material can be affected via dislocation/microstructure interactions by microstructural changes resulting from phenomena such as deformation-induced transformation (e.g., martensite formation in metastable austenitic stainless steels), mechanical twinning (e.g., in intermetallic phases), deformation-induced precipitation (e.g., in solution-annealed alloys) and coarsening (e.g., in precipitation-strengthened materials).

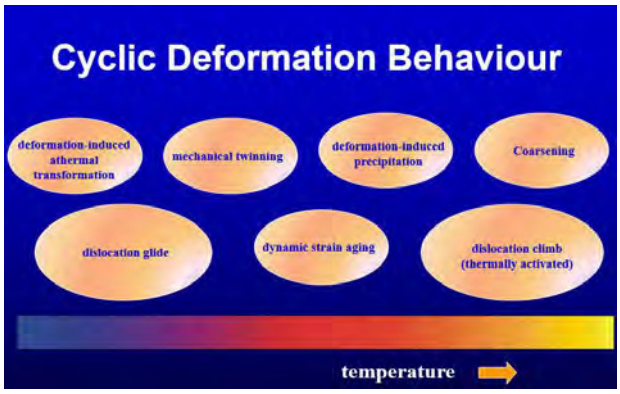

Fig. 5. Examples for the effect of temperature on the cyclic stress-strain behaviour.

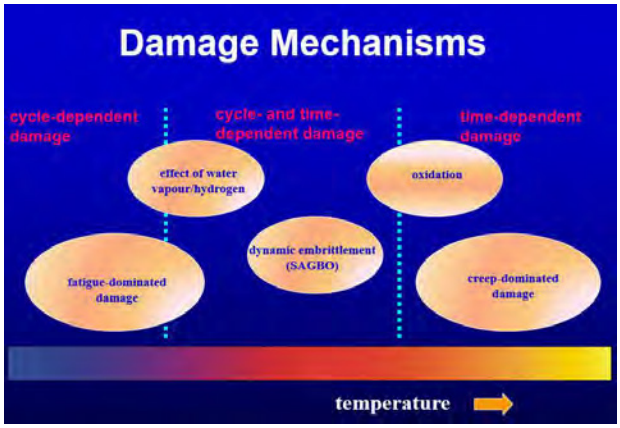

Fig. 6. Examples for the effect of temperature on the relevant damage mechanism.

A similar strong dependence on temperature exists for the dominant damage mechanism which is responsible for isothermal fatigue life of a material. Figure 6 represents a small selection of possible mechanisms. With increasing temperature a shift from cycle-dependent damage to time-dependent damage occurs. The last one is mainly a consequence of environmental effects and creep. Some materials are known to be prone to specific damage contributions such as hydrogen effects in the case of titanium alloys at moderate temperatures or dynamic embrittlement, often also termed stress-assisted grain boundary oxidation (SAGBO), of polycrystalline Ni-base superalloys.

As a prominent example for a temperature influence, the effect of DSA on cyclic stress-strain response and fatigue life N_f of AISI 304L is shown in Fig. 7 [16]. DSA leads to an increase of the maximum and saturation stress amplitude in an intermediate temperature range observed in tests carried out at a constant plastic strain amplitude of 0.5%. As a direct consequence of this stress amplitude raise the cyclic life drops in the corresponding temperature range, before creep damage reduces N_f further (see Fig. 8).

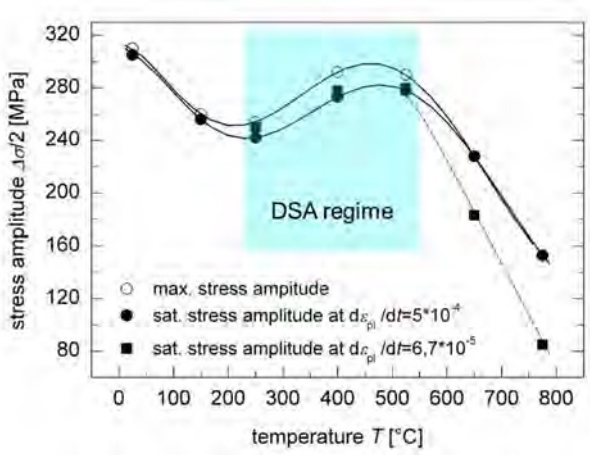

Fig. 7. Influence of DSA on the maximum and saturation stress amplitude of AISI 304L cyclically loaded at a plastic strain amplitude of 0.5%.

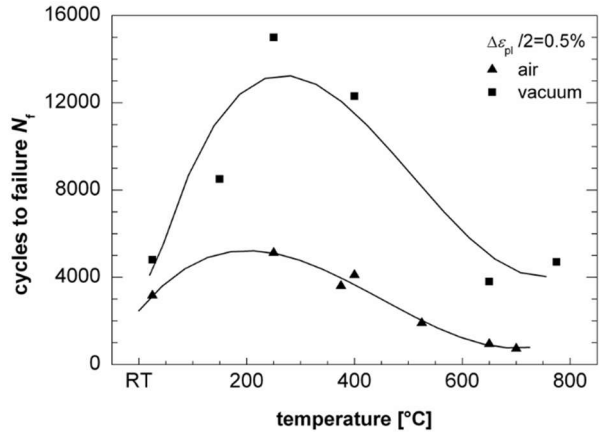

Fig. 8. Influence of DSA on fatigue life of AISI 304L obtained in air and in vacuum at a plastic strain amplitude of 0.5%.

The reason for the strong change in the cyclic stress-strain response of the austenitic stainless steel is the impeding effect of point defects on the dislocation mobility in the intermediate temperature range. This interaction of dislocations with point defects manifests itself in a tremendous change in the dislocation arrangement, as shown in the TEM micrographs of Fig. 9. While below the DSA temperature range, dislocations form cells, which is a wavy-slip-type structure typically of high plastic strain amplitudes, DSA leads to a planar

dislocation arrangement. At sufficiently high temperature, the effect of DSA vanishes and a cell arrangement with a tendency to form subgrains prevails.

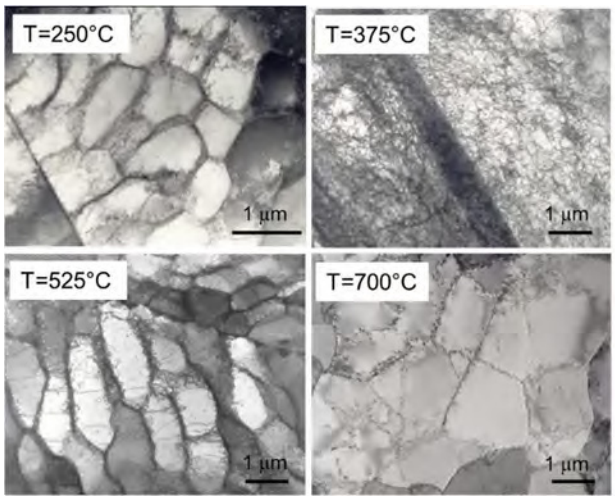

Fig. 9. Change of the dislocation arrangement with temperature: wavy arrangements above and below the temperature range of DSA, planar arrangement in the DSA range.

At temperatures above 650°C and/or slow cyclic plastic strain rates, austenitic stainless steels are prone to a change of the fatigue crack propagation from a transgranular to a intergranular type (see Fig. 10). This transition leads to a strong increase of the crack growth rate.

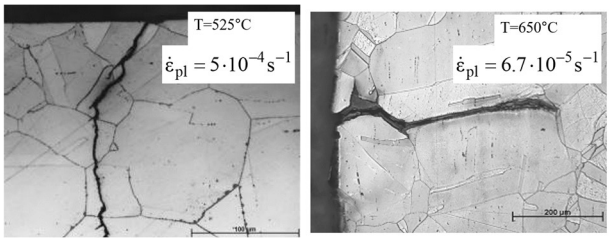

Fig. 10. Change from transgranular to intergranular fatigue crack propagation in AISI 304L austenitic steel.

Two examples for microstructural instabilities affecting strongly the cyclic stress-strain response are shown in Fig. 11 und Fig. 12. Figure 11 refers to the near-α Ti alloy IMI 834. At temperature exceeding about 600°C the boundaries in the colonies of the lamellar grains of the bimodal microstructure disintegrate leaving behind silicides which mark the former boundaries.

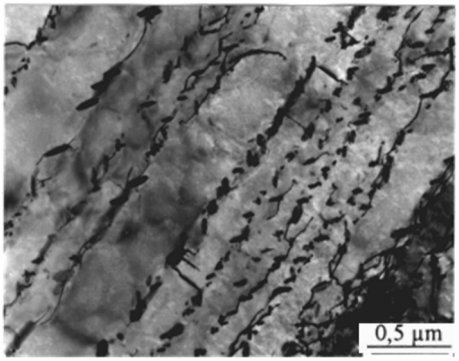

Fig. 11. Disintegration of lamellar boundaries in IMI 834

In γ-TiAl alloys the microstructural stability is limited to about 800°C. Above this temperature the lamellar structure is destroyed by a kind of dynamic recrystallization (see Fig. 12) reducing the strength strongly.

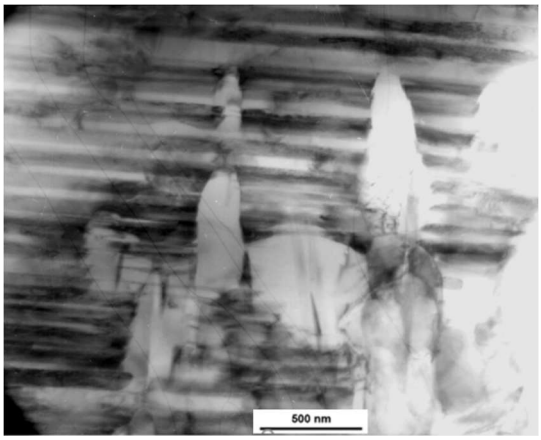

Fig. 12. Recrystallization in TiAl-based alloy TNB-V2.

Figures 13 und 14 [8] show typical examples for crack initiation sites as observed on IMI 834 after cyclic deformation at low and high temperature, respectively. Up to a testing temperature of about 400°C, most cracks are formed within the primary α grains (Fig. 13). At higher magnification, it becomes apparent that cracks initiate along planar slip bands.

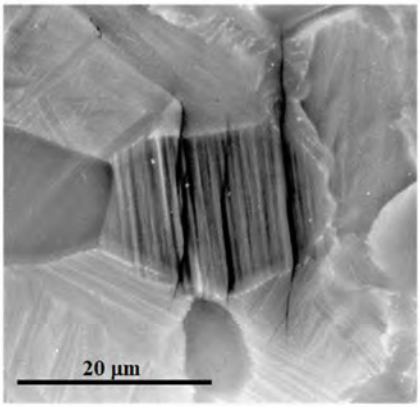

Fig. 13. Crack initiation in IMI 834, isothermal fatigue at 400°C.

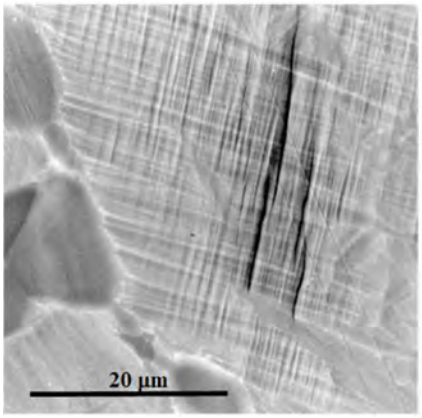

Fig. 14. Crack initiation in IMI 834, isothermal fatigue at 600°C.

The few fatigue cracks which were found in the primary α grains at T=600°C seem to become non-propagating as soon as they reach the grain boundary. The cracks now form in the transformed α grains (the prior β grains) and

seem to grow unhindered (Fig. 14). A possible explanation for this change in the crack initiation mechanism is a transition in slip mode from planar to wavy which occurs at around 600°C.

However, this changes seems to be much less important than the change in the relevant environmental effect. Titanium alloys are known to be susceptible to hydrogen (e.g., resulting from the moisture in air) in particular in the intermediate temperature range. The detrimental effect of oxidation is more pronounced at high temperature, since the TiO_2 surface layer formed is no longer stable. Rather, the oxide is dissolved in the material leading to a brittle oxygen-enriched surface zone, which is referred to as α-case.

This temperature effect must be considered by an appropriate model concept as shown in Fig. 15. The straight line represents the correlation between the maximum stress established in cyclic saturation of plastic-strain-controlled fatigue tests performed at a plastic strain amplitude of 0.2% with the number of cycles to failure. The full data points refer to corresponding tests carried out in air. Modelling the effect of hydrogen explains only the fatigue life reduction at temperatures up to about 400°C. To explain the reduced life at higher temperatures oxidation has to be taken into account. The combination of both effects allows a very satisfactory fatigue life assessment (see [8] for model details).

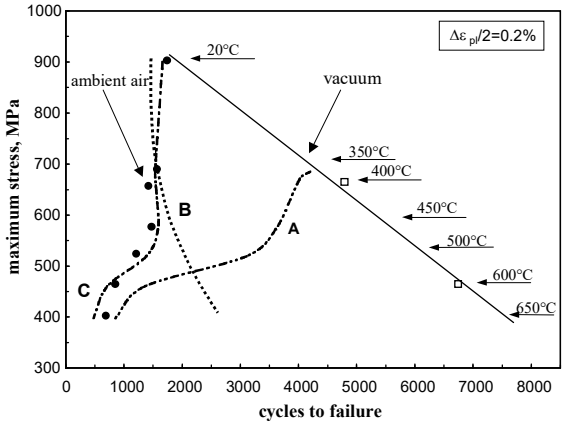

Fig. 15. Effect of oxidation (dashed line A) and hydrogen embrittlement (dotted line B) on cyclic life of IMI 834. The combination of both effects (line C) leads to a reasonable life assessment for isothermal conditions.

The considerations and supporting examples shown in this chapter clearly demonstrate that before dealing with TMF a sound understanding of the isothermal behaviour has to be developed. This behaviour forms the reference related to which the effects arising from the varying temperature of TMF can be identified. Hence, this sound basis obtained from extensive isothermal testing is a must for any rational consideration of TMF.

3.2 Peculiarities of the TMF behaviour

The strong effect of temperature on both the cyclic stress-strain behaviour and the relevant damage mechanism documents that already under isothermal conditions a high-temperature fatigue life assessment is very complex. The complexity increases immensely, if the temperature is continuously varied as is the case under TMF conditions.

A first important step in an identification of the TMF-specific behaviour is the knowledge of the so-called pseudoisothermal TMF (PI-TMF) behaviour. The PI-TMF behaviour predicts the cyclic stress-strain response which would exist, if the material behaves at each temperature in a TMF cycle identical to the corresponding isothermal case. A comparison of the PI-TMF behaviour with the experimentally determined behaviour (e.g., in form of the hysteresis loops) reveals the differences and provides valuable information on the TMF-specific mechanisms.

For the calculation of PI-TMF behaviour viscoplastic constitutive equations can be used. In the investigations carried out in the author's research group a multi-component behaviour approach is favoured, since all necessary model parameters can be determined from isothermal stress-strain hysteresis loops. The basic concept was proposed by Masing already in 1923 [17] assuming that a material behaves like a composite consisting of a parallel arrangement of ideally elastic-plastic elements which differ in yield stress. The distribution function of these microscopic yield stresses is a kind of a mathematical representation of the microstructure and can be determine by a double differentiation of one single stress-strain branch of a hysteresis loop (details can be found in ref. [18]).

The expansion of this multi-component approach to TMF is described in ref. [19] and requires the following procedure:

- The yield stress distribution function must be determined from isothermal tests at various temperatures.
- The distribution function must be interpolated regarding the temperature.
- The distribution function must then be transformed into a discrete distribution (e.g., 30 elements)
- The TMF loading situation must be determined in terms of $T(t)$ and $\varepsilon(t)$.
- The stress-strain relationship can then be calculated stepwise by
    - stepwise changing temperature and strain in each element and
    - calculating the total stress after each step from the individual stresses of all elements.

Figure 16 shows calculated hysteresis loops for two IP TMF tests with temperature ranges falling partially in the DSA regime in a representation of stress versus temperature. The calculated PI-TMF loops are compared with the corresponding experimental hysteresis loops. The course of the maximum and minimum saturation stress also plotted shows the DSA-induced increase in strength in the intermediate temperature range.

In this temperature regime of DSA, the extreme values of the hysteresis loops coincide, while outside this regime the experimental hystereses document a higher strength as observed in the isothermal tests and predicted by the PI-

TMF loops. The reason for this behaviour is illustrated in Fig. 17. TMF loading leads to typical dislocation arrangements which were not found for isothermal conditions (compare Fig. 9). These arrangements consist of dislocation-poor channels embedded in a wall structure (Fig. 17a) or a labyrinth-type arrangement (Fig. 17b).

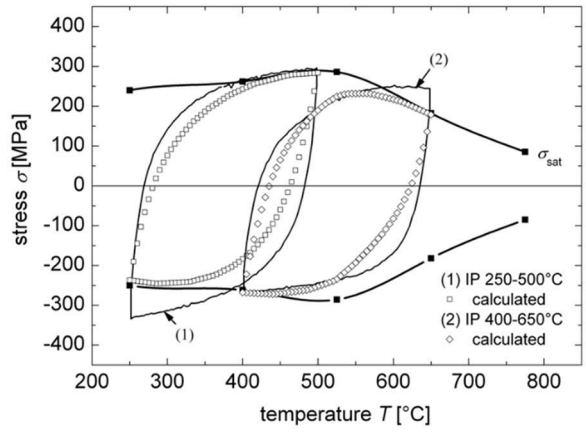

Fig. 16. Comparision of the isothermal and the athermal (TMF) stress strain response for AISI 304L**.**

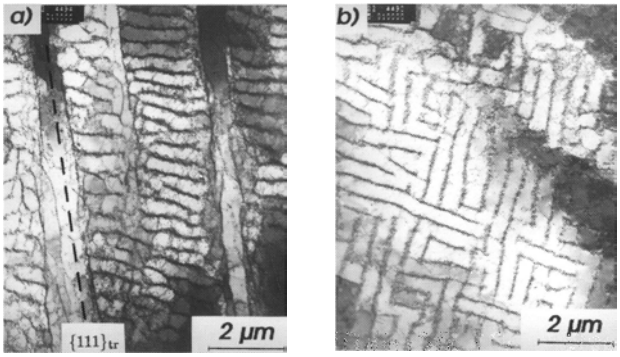

Fig. 17. Typical dislocation arrangements found exclusively after TMF loading: a) dislocation channels and walls, b) labyrinth-type arrangement.

Additional tests, where TEM samples were prepared after different numbers of loading cycles from specimens, which were fatigued under identical TMF conditions, indicate that despite the varying temperature a steady state condition is established in the microstructure. That means that the change from cycle to cycle is very small or is even negligible.

In order to understand the reason for the deviation of the TMF stress-strain response from the one of isothermal fatigue, tests were performed with block-wise constant temperature. Figure 18 shows the answer of AISI 304L to a sudden temperature change from 400°C to 650°C during fatigue testing at a constant plastic strain amplitude of 0.5%. As mentioned above the first temperature is in the DSA regime and a planar type of dislocation arrangement is formed. The increase to 650°C leads to a stress amplitude which is significantly higher than the corresponding stress amplitude of the isothermal test at this temperature (dashed line). Therefore, it can be concluded that the dislocation arrangement formed after the temperature change is strongly affected by the DSA prehistory. The consequence of this observation is that if TMF modelling deals with conditions where the DSA temperature range is passed through the required stress-strain data should be determined in temperature-change tests instead of IF testing (see details in [16]). Figure 19 compares such a calculated hysteresis loop with the corresponding experimental loop. The agreement is very reasonable documenting that the deviations depicted in Fig. 16 result from the TMF-specific dislocation arrangement.

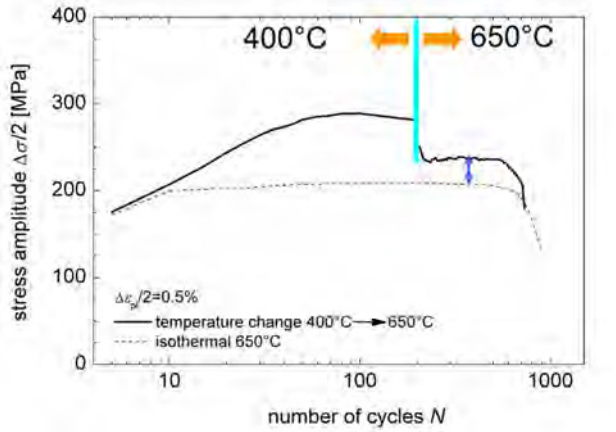

Fig. 18. Cyclic stress-strain response of AISI 304L to a change of temperature while keeping the other parameters constant.

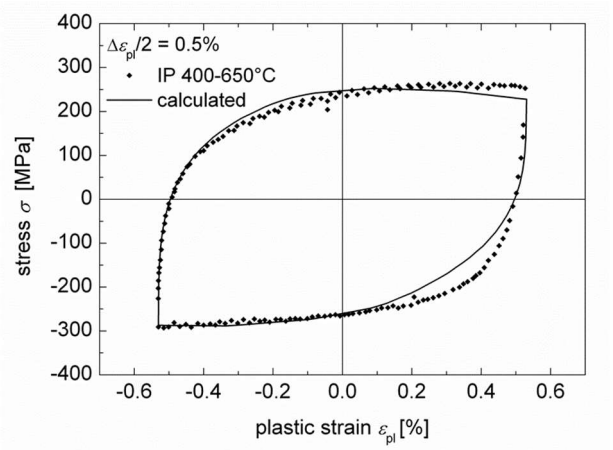

Fig. 19. Comparison of a calculated and an experimental TMF hysteresis loop. The calculation was done using the stress amplitude from temperature change tests.

The formation of a TMF-specific microstructure was also observed for the near-α Ti alloy IMI 834. This material shows in isothermal tests a transition from a planar dislocation arrangement to a wavy one at around 600°C. As a consequence, the dislocation arrangement becomes more wavy, if the maximum temperature applied in the cycle of a TMF test exceeds 600°C. A comparison of the microstructures formed in two TMF tests with a minimum temperature of 400°C and a maximum temperature of 600°C or 650°C is shown in Fig. 20.

The existence of a TMF-specific microstructure manifests itself in a different stress amplitude after the change from TMF to isothermal conditions [20]. Simply by stopping the temperature variation and holding the temperature constant, such a change can be carried out. Figure 21 shows a test, where the minimum temperature (400°C) of the TMF test was kept constant in the

isothermal part of the fatigue experiment. A comparison with the corresponding isothermal test clearly shows that the TMF part establishes a stable dislocation arrangement that is harder at low temperatures than the corresponding isothermal microstructure.

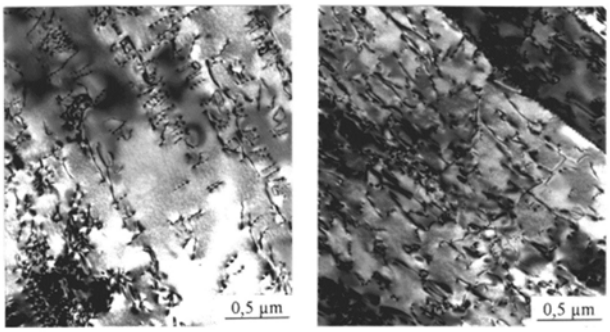

Fig. 20. Comparison of the dislocation arrangements in IMI 834 after TMF testing with a temperature range of 400°C-600°C (left) and 400°C-650°C (right). The slight increase of the maximum temperature of the TMF cycle promotes a wavier microstructure.

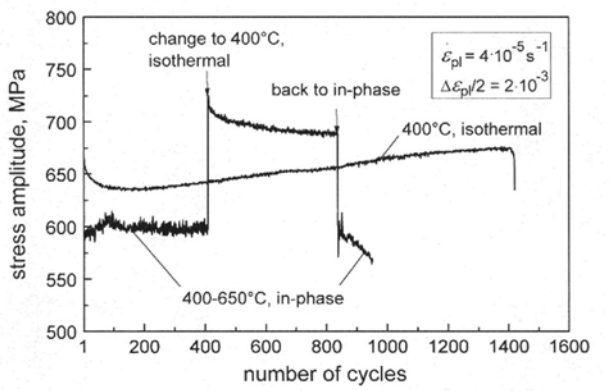

Fig. 21. Cyclic stress-strain response of a test carried out with a change from TMF to isothermal conditions. The higher stress amplitude in the isothermal part of the change test documents the higher strength of the dislocation arrangement established under TMF conditions.

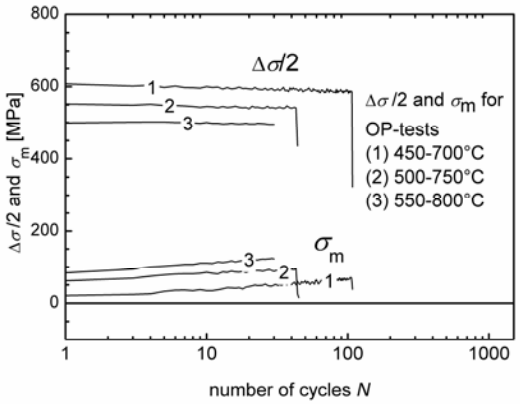

Fig. 22. Change of mean stress σ_m and stress amplitude $\Delta\sigma/2$ with number of loading cycles during OP-TMF testing of the TiAl alloy γ-PX.

In the case of the near-γ TiAl alloys a very stable microstructure was observed in the temperature range of interest. No significant differences between the isothermally formed dislocation arrangements and the corresponding TMF arrangements were detected. Consequently, the isothermal fatigue behaviour is characterized by a pronounced cyclic saturation. This holds also true under TMF conditions with respect to the stress amplitude. However, a mean stress develops continuously as seen in Fig. 22 for OP-TMF. The non-isothermal conditions lead to cyclic softening at high temperatures and (slight) cyclic hardening at low temperatures resulting in a mean stress in OP and IP testing which is positive (tensile) and negative (compressive), respectively. In particular, the positive mean stress developing during OP conditions strongly deteriorates TMF life as will be discussed in the next chapter.

As part of the answer to the basic question of TMF life predictability addressed in this paper, the conclusion from these (and many other existing) examples is that a thorough study of the specifics of TMF is indispensable in order to select the suitable approach for TMF life assessment. Hence, at least some TMF tests must be carried out, and the testing parameters should be chosen in such a way that they match the service conditions closely.

3.3 TMF life assessment and immanent brittleness

Most of the models reported in the literature, which are used for TMF life prediction, are connected in some way to the hysteresis loop or the deformation energy density. This holds true for many empirical approaches but also for most fracture mechanics concepts suitable for high temperatures. An application of these concepts is very problematic, if the material considered behaves brittle. Brittle behaviour is in this context synonymic to a negligible fraction of life spent in crack propagation, and hence the stage of crack initiation is more important. Unfortunately, crack initiation is a very complex process starting from an atomic level, and despite much research effort the process still detracts from a mechanism-based and quantitative description.

Fatigue life results under TMF loading conditions are compared with isothermal fatigue life data in Fig. 23 for the near-γ TiAl alloy γ-PX. TMF data is plotted as a function of the maximum temperature of the corresponding TMF cycle. The fatigue life of IP tests is approximately twice the life observed in isothermal LCF tests performed at the highest temperature of the TMF test. One reason for higher fatigue lives under IP conditions is the negative mean stress as discussed before. On the other hand, an oxide layer grows at high temperature on the specimen surface in the tension part. Apparently, the tension loading is not crucial for oxide scale cracking or spalling. For this reason, cracks initiate slowly.

In contrast, OP loading conditions reduce fatigue life tremendously. The fatigue life decreases at least by a factor of 5. The short TMF life in OP mode can be attributed to the accelerated oxidation-induced crack initiation during OP testing. The oxide layer mainly formed at high temperatures becomes brittle at lower

temperatures. In the low temperature part of the cycle (tension) the oxide cracks easily and hence, promotes crack initiation. Once formed, cracks lead to failure quickly, because of the brittleness of the alloy at low temperatures (tension). This manifests itself in very different fracture surfaces of OP and IP TMF tests as shown in Fig. 24.

A comparison of the results of the OP tests in vacuum (Fig. 23) with isothermal air tests documents that the positive mean stress shown in Fig. 22 reduces cyclic life strongly. However, the effect of environment leads to a further tremendous life reduction.

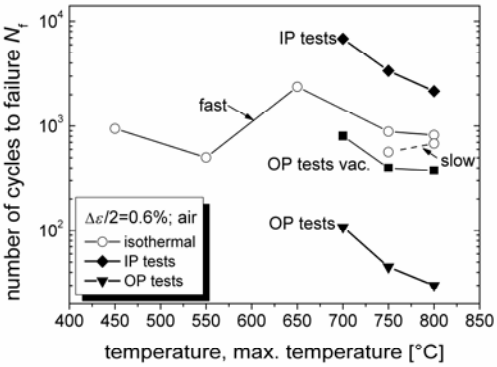

Fig. 23. Fatigue life data of the near-γ TiAl alloy γ-PX as a function of testing temperature and maximum temperature of isothermal and non-isothermal conditions, respectively.

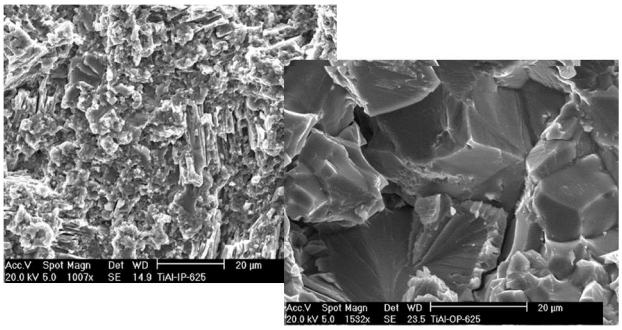

Fig. 24. Fracture surface from IP (left) and OP (right) TMF tests performed at a strain amplitude of 0.6% and a temperature range of 550°C-750°C.

The pronounced susceptibility of the cyclic life of the near-γ TiAl alloys to mean stresses demands the use of a damage parameter which explicitly considers this effect. The concept of Ostergren [21] provides a simple empirical, energy-based approach, which holds true for the isothermal tests. In order to consider the effect of oxidation, temperature and frequency, an expansion of the model is necessary, which can be obtained by implementing a combination of the frequency-modified Ostergren model [22] with the oxidation damage model of Antolovich [23].

If this concept is applied to describe TMF life on the basis of the isothermal data, the match is very poor indicating that TMF damage evolution deviates strongly from the isothermal behaviour (see Fig. 25). IP TMF life is conservatively predicted, while the experimentally observed OP TMF life is much shorter than expected from the assessment. Hence, as already stated in the beginning of this section, a sufficient ductility of the material considered is a fundamental requirement for a successful application of current TMF life prediction methodologies.

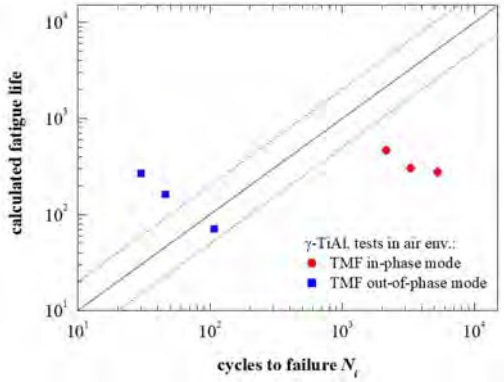

Fig. 25. Conservative and non-conservative prediction of IP TMF and OP TMF, respectively.

However, recently a new damage parameter could be developed and introduced, which seems to capture the strong effect of mean stress, oxidation and TMF phasing for the brittle TiAl-based alloys in such a way that the unified description of isothermal and TMF life works satisfying [24].

In this life assessment model, a damage parameter P was defined strongly emphasizing the influence of mean stress σ_m. This parameter P (similar to the one suggested by Buchholz in his Ph.D. thesis (Dresden 2012)) includes the temperature as a variable quantity and contains only one fitting parameter α:

$$P = \frac{1}{2}\left(\frac{\sigma_{tlrp}}{R_{p0.2}(T_{tlrp})} + \frac{\sigma_{clrp}}{R_{p0.2}(T_{clrp})}\right) + \left(\frac{\sigma_m}{R_{p0.2}(T_m)}\right)^{\alpha} \quad (1)$$

The subscripts *tlrp*, *clrp* and *m* correspond to the tensile load reversal point, the compression load reversal point and the mean value, respectively. All these parameters can be calculated from the above described multi-component model by means of the simulation of the hysteresis loop considering the changes deformation behaviour.

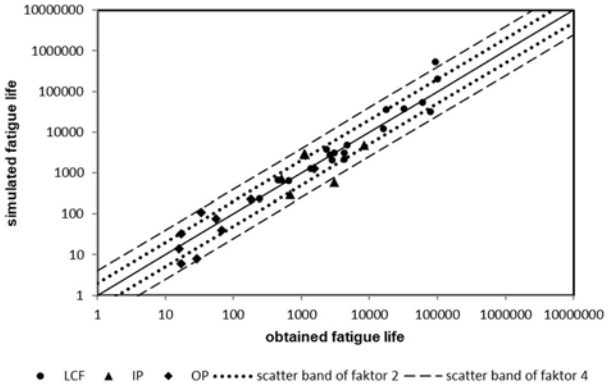

Fig. 26. Comparison of simulated and observed lifetimes for LCF, IP TMF and OP TMF.

Finally, the correlation between this damage parameter and the number of cycles until failure is given by a power law:

$$P = A \cdot N_f^{\,b} \quad (2)$$

Figure 26 shows a comparison between the simulated and the observed life for both LCF and TMF (IP and OP) conditions. Most data points lie within the scatter band of factor 2.

3.3 Successful mechanism-based TMF life prediction

From the previous sections it should have become clear that a successful development and application of a life prediction model for TMF conditions requires a thorough experimental characterization of both the isothermal and non-isothermal fatigue behaviour of the material considered and a mechanism-based and realistic theoretical approach with respect to damage evaluation. Unfortunately, each material has its specialities so that a generally applicable methodology cannot be expected. Rather an individual consideration which is laborious and time-consuming must be carried out. Selected examples are given in this section to shed some light on the required line of actions.

Fracture mechanics methods are a suitable means of describing fatigue life both for isothermal and thermomechanical conditions (see ref. [8] for details). However, the concepts must be selected carefully such that they relate closely to relevant damage mechanisms and microstructural processes. Hence, no fracture mechanics damage parameter is *a priori* qualified. Rather extensive testing in combination with detailed microstructural and fractographic studies must be carried out, before an appropriate concept can be selected. This approach is illustrated for the alloy X8019/12.5$_p$ in Figs. 27, 28 and 29.

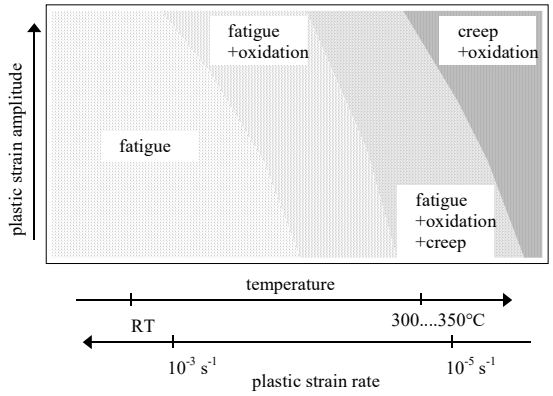

Fig. 27. Map of the damage regimes as a function of plastic strain amplitude (ordinate) and temperature or plastic strain rate (abscissa) for the particle-reinforced aluminium alloy X8019/12.5$_p$.

Figure 27 presents a map which shows the regimes of plastic strain amplitude (ordinate) and temperature or plastic strain rate (abscissa) where damage can be attributed to fatigue, creep, oxidation or combinations of these damage types. On the basis of such a map, which resulted from metallographic inspection of correspondingly tested samples, a suitable damage parameter can be chosen and applied to the respective loading parameter regime (Fig. 28). In the case of TMF, adaptation of these concepts to non-isothermal conditions requires even more consideration in order to deduce simplifications which enable the adaptation but are also reasonable from a mechanistic point of view.

In the case of the dispersoid-strengthend aluminum alloy X8019 in SiC particle-reinforced as well as non-reinforced condition the transformation of the cyclic stress-strain behaviour and the damage evolution from isothermal to non-isothermal conditions appears to be justified without any major adaptations. This is a consequence of a stable microstructure, which leads to a very strong dislocation-particle interaction irrespective of the testing mode (IF, IP-TMF or OP-TMF). Hence, no appreciable difference in the dislocation arrangement is observable. Moreover, the temperature range of the intended application of these alloys is small so that environmental effects are only of minor significance.

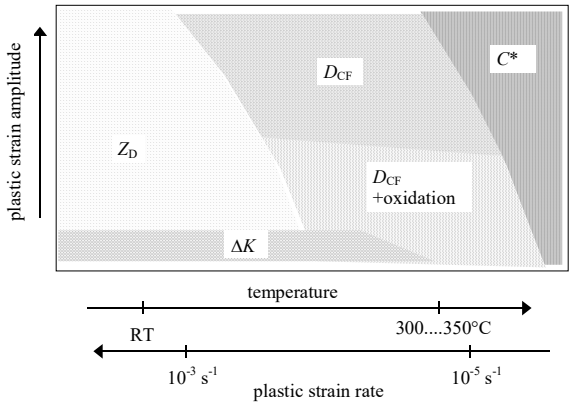

Fig. 28. Schematic map representing the regimes of the respective life prediction concepts deduced from Fig. 26 for X8019/12.5$_p$.

Figure 29 compares the results of the fracture-mechanics-based fatigue life assessment with the experimentally determined number of cycles to failure. The predictive capability is very satisfactory both for isothermal and thermomechanical conditions.

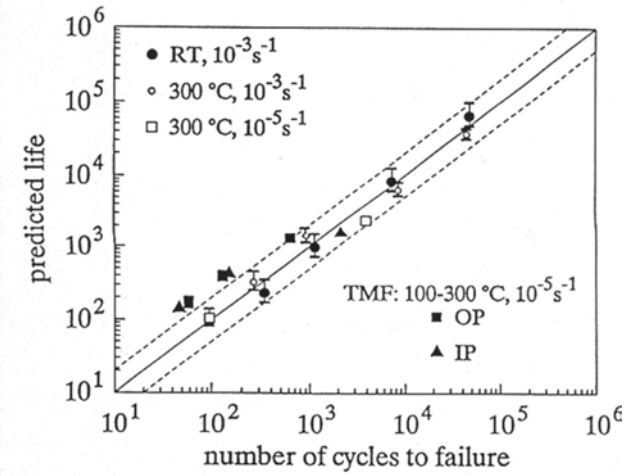

Fig. 29. Comparison of experimentally obtained and calculated IF and TMF lives of X8019 at plastic strain rates of 10^{-5} s^{-1} and 10^{-3} s^{-1}.

It has been described already above and depicted in Fig. 15 that the isothermal fatigue life of the near-α Ti alloy IMI 834 is strongly influenced by environmental effects. The fatigue lives in vacuum are reasonably well predicted with the assumption of pure fatigue. The curves labelled A and B in Fig. 15 represent the calculated results for dry air and humid argon environment, respectively. The linear combination of both environmental damage

contributions yields satisfactory results over the whole temperature range (curve C).

The consideration of environmental effects on fatigue life in TMF is more complicated and demands additional assumptions. Hydrogen embrittlement was assumed to be negligible in the case of IP TMF as stresses are mostly compressive in the low-temperature part of the cycle. Consequently, oxidation was the only environmental effect considered for IP-TMF. By contrast, both environmental degradation mechanisms were accounted for to predict N_f of OP-TMF tests. Oxygen uptake was assumed to be not affected by the sign of the stress. Since high tensile stresses coincide with low temperature in OP-TMF, hydrogen embrittlement must be expected due to the reaction of the alloy with water vapour. Figure 30 compares the experimentally observed TMF lives of IP and OP tests at two values of the plastic strain amplitude with the results of the prediction calculation. As can be seen, all data points lie within a ±2 scatter band.

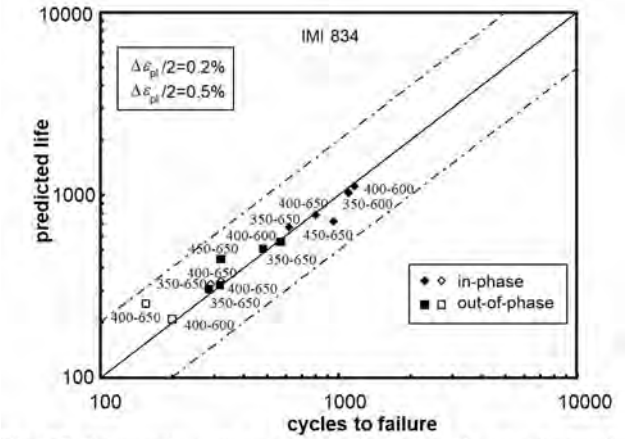

Fig. 30. Comparison of experimentally obtained and calculated lives for IMI 834 under TMF conditions at plastic strain amplitudes of 0.2% (full symbols) and 0.5% (open symbols). Temperature range of test is given next to symbol.

The behaviour auf the austenitic stainless steel of type AISI 304L has been described in detail above in terms of the temperature dependence of the isothermal stress-strain response and the TMF-specific implications. AISI 304L shows a cyclic stress-strain behaviour under TMF conditions that deviates characteristically from that observed under isothermal conditions. This phenomenon can be attributed to the occurrence of dynamic strain aging. The significance of environmental effects is moderate for the austenitic stainless steel. The main damage contribution through the interaction with the surrounding air as compared to vacuum is the preferential grain boundary oxidation leading to a premature crack initiation. This process is most important at high temperature and under conditions where the internally developing creep damage is negligible. Hence, OP loading with high maximum temperature promotes environmental effects. In principle, the influence of air is similar for isothermal and thermomechanical conditions so that isothermally obtained life data can be applied to TMF life assessment.

The multi-component model introduced in chapter 3.2 helps to identify the TMF-specific behaviour and can easily be expanded in such a way that these effects are considered. For this purpose, additional fatigue tests applying temperature changes were carried out to capture the effect of cyclic deformation in the temperature regime of dynamic strain aging.

For high maximum temperatures of the TMF cycle, superimposed dwell times or very low strain rates, creep and relaxation have to be taken into account as important contributions to the deformation of AISI 304L. By means of a simple relaxation law based on Norton's power law creep equation, the change of the yield strength resulting from relaxation was taken into account in each elementary volume leading to a very reasonable prediction of the stress-strain behaviour.

Three different approaches were used to predict TMF life of AISI304L solely from isothermal cyclic stress-strain and life data [10]. Here, a phenomenological energy-based approach and a damage mechanics concept [25] are briefly introduced, while a fracture mechanics method is described in ref. [26].

A well-known damage parameter for high-temperature cyclic loading conditions is the creep-fatigue damage parameter D_{CF} proposed by Riedel [27]. This parameter can be considered to describe the deformation energy density per loading cycle, and therefore the respective life assessment approach belongs to the class of phenomenological, energy–based life prediction concepts. The definition of D_{CF} as used in this study is given in Eq. (3).

$$D_{CF} = 2.9\frac{(\Delta\sigma)^2}{2E} + 1.9\,\Delta\sigma\left(\Delta\varepsilon_{pl} + \Delta\varepsilon_{cr}\right)\left(1+\frac{\Delta\varepsilon_{cr}}{\Delta\varepsilon_{pl}}\right)^{(1+n)} \quad (3)$$

Here, n is the cyclic hardening exponent, and $\Delta\sigma$, $\Delta\varepsilon_{pl}$ and $\Delta\varepsilon_{cr}$ are the ranges of stress, plastic strain and creep strain per cycle. $\Delta\varepsilon_{cr}$ can either be determined by means of additional creep tests or by comparing hysteresis loops observed at different plastic strain rates. According to the last-mentioned method, the creep strain range is determined as the difference of the total inelastic strain range observed at the plastic strain rate of interest and the plastic strain range obtained during cycling at high strain rates (no creep contribution) applying the same stress range.

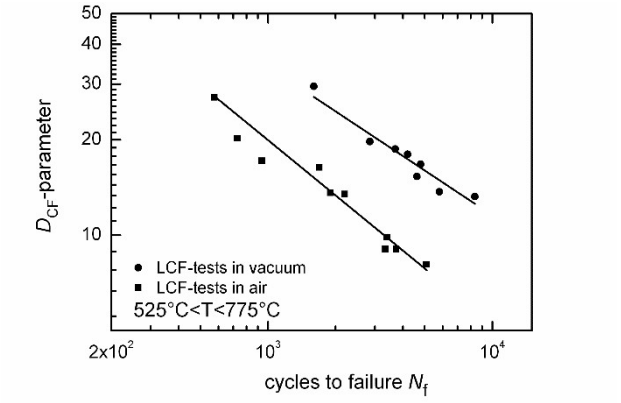

Fig. 31 Correlation between the number of cycles until failure of isothermal tests carried out in air and in vacuum and the corresponding value of the D_{cf} damage parameter.

Figure 31 shows that the parameter D_{CF} correlates nicely with the isothermal fatigue life data. However, two separate lines exist for the two environments considered. Clearly a simple power law describes the relation of D_{CF} with N_f in each case.

$$N_f = L\left(D_{CF}\right)^{-q} \tag{4}$$

The constants L and q can directly be taken from the lines shown in Fig. 31 and their values contain implicitly the effect of environment on fatigue life.

The so-called *loop reversion method* after Nitta et al. [28,29] was used to determine the creep strain range for the IP-TMF cycles, while no creep contribution was assumed for OP cycling. Loop reversion means that the descending branch of the IP TMF hysteresis loop is mirrored, shifted to a common origin and compared with the ascending branch. The creep strain range is defined as the difference between the inelastic strain of the ascending branch at the stress of T_{max} and the plastic strain taken from the mirrored branch at the same stress (see Fig. 32).

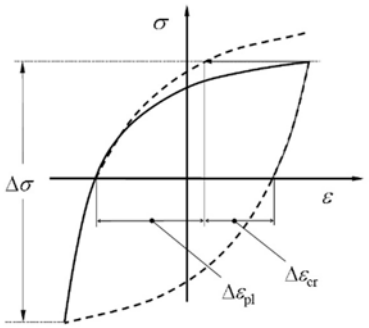

Fig. 32. Schematic representation of the "loop reversion method" used to determine the creep strain contribution of in-phase TMF loading.

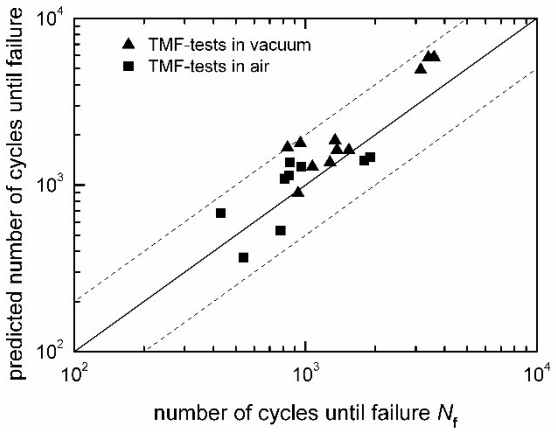

Fig. 33. Predicted TMF life calculated on the basis of the correlation between D_{cf} and N_f found for isothermal conditions (Fig. 31) in comparison to the experimentally observed TMF life data.

TMF life was calculated using the constants L and q from the isothermal tests. Figure 33 compares the predicted number of cycles until failure with the experimentally determined ones. Taking the complexity of TMF loading and the simplicity of the model used into account, the agreement must be considered as very satisfactory. All data points lie within a band of a maximum deviation of a factor of two (dashed lines in Fig. 33).

The damage mechanics model used is based on an equation for the increase of the damage state variable ω proposed by Lemaitre and Chaboche [30]:

$$\mathrm{d}\omega = \left\{ \frac{(1-\omega)^{-\lambda}}{(\lambda+1)\cdot N_c} + \frac{\left[1-(1-\omega)^{\beta+1}\right]^{\alpha}}{(\beta+1)\cdot N_f \cdot (1-\alpha)\cdot (1-\omega)^{\beta}} \right\} \cdot \mathrm{d}N \tag{4}$$

The first term in braces represents the creep contribution to damage evolution, while the second term results from fatigue. λ denotes the creep damage tolerance factor and was determined from creep data according to

$$t_r = \frac{1}{\lambda+1} \cdot \frac{\sigma^{-n}}{A_0} \tag{5}$$

using the time until rupture t_r under creep conditions at creep stress σ and the two parameters stress exponent n and coefficient A_0 of Norton's creep law.

N_c represents the life in terms of the number of cycles to failure as a consequence of creep damage and can be calculated for cyclic loading from the cycle period t_{cyc}, the apparent activation energy of steady state creep Q, the stress exponent n and the coefficient A_0:

$$\frac{1}{N_c} = (\lambda+1) \int_0^{t_{cyc}/2} \frac{\sigma(t)^n}{A_0} \cdot \exp\left(\frac{-Q}{RT}\right) \mathrm{d}t \tag{6}$$

The constants α and β of the fatigue term in Eq. (4) were obtained from the isothermal fatigue life data, separately for air and vacuum [31]. Furthermore, the number of cycles to failure for plain fatigue N_f was calculated according to Ostergren [21]:

$$N_f = L_1 \cdot \left(\Delta\varepsilon_{pl} \cdot \sigma_{max}\right)^{-\eta} \cdot \nu^{1-k} \tag{7}$$

σ_{max} denotes the maximum stress and ν the test frequency. The constants L_1, η and k were deduced from the isothermal fatigue lives, separately for the tests performed in vacuum and air. The values, which were obtained, are L_1=1166, η=-1.86, and k=0.76 for vacuum [13] and L_1=3577, η=-1,04, and k=0,51 for air [11].

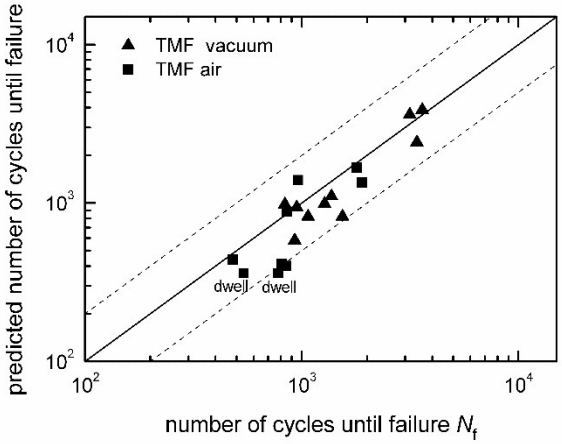

Fig. 34. Predicted TMF life calculated on the basis of the damage mechanics model according to Eqs. (4-7) using solely isothermal results in comparison to the experimentally observed TMF life data.

Figure 34 compares the experimentally observed TMF life data with the predicted lives. A very reasonable agreement can be stated irrespectively of plastic-strain/temperature phasing (IP or OP) for both the vacuum tests and air tests. It is worth noting that also the effect of superimposed dwell times (see data points labelled "dwell") leads to a conservative prediction.

3 Conclusions

From the results presented as examples to illustrate the variety of behavioural patterns of metallic structural materials under isothermal and non-isothermal conditions, the conclusion can be drawn that the following prerequisites should be fulfilled, in order to reach a reasonable predictive capability of TMF life assessement on the basis of mainly isothermal data:

- The mechanisms relevant for isothermal fatigue must be understood as a function of temperature in the temperature range of TMF loading.
- The specifics of the TMF behaviour both in terms of cyclic stress-strain response and damage evolution must be known and taken into account.
- The material considered should exhibit sufficient cyclic plasticity; otherwise the brittleness requires a particular and material-specific consideration.
- The method used for TMF life assessment must be selected on the basis of the relevant damage mechanisms.

Deutsche Forschungsgemeinschaft (DFG) is gratefully acknowledged for the financial support of the studies this article is based on.

References

1. H.L. Bernstein, in: *Low-cycle fatigue and life prediction, ASTM STP 770*, C. Amzallag, B.N. Leis, P. Rabbe (Eds.), American Society for Testing and Materials, Philadelphia, PA, 105 (1982)
2. F. Ellyin *Fatigue damage, crack growth and life prediction* (Chapman & Hall, London, 1997)
3. R. Danzer, *Lebensdauerprognose hochfester metallischer Werkstoffe im Bereich hoher Temperaturen* (Gebr. Borntraeger, Berlin, 1988)
4. H.J. Maier, R.G. Teteruk, H.-J. Christ, Materials at High Temperatures **19**, 9 (2002)
5. A. Nagesha, M. Valsan, R. Kannan, K. Bhanu Sankara Rao, V. Bauer, H.-J. Christ, Intern. Journal of Fatigue **21**, **636** (2009)
6. R. Zauter, F. Petry, H.-J. Christ, H. Mughrabi, in: *Thermomechanical behavior of materials, ASTM STP 1186*, H. Sehitoglu (Ed.), American Society for Testing and Materials, Philadelphia, PA, 70 (1993)
7. H.-J. Christ, A. Jung, H.J. Maier, R. Teteruk, SADHANA **28**, 147 (2003)
8. H.-J. Christ, R. Teteruk, A. Jung, H J. Maier, in: *Thermomechanical Fatigue Behavior of Materials, 4th Volume, ASTM-STP 1428*, A. McGaw, S. Kalluri, J. Bressers, S. D. Peteves (Eds.), American Society for Testing and Materials, West Conshohocken, PA, 145 (2003)
9. H.-J. Christ, Mater. Sci. Engng A, **A468-470**, 98 (2007)
10. V. Bauer, H.-J. Christ, *Intermetallics* **17**, 370 (2009)
11. V. Bauer, *Verhalten metallischer Konstruktionswerkstoffe unter thermomechanischer Belastung - Experimentelle Charakterisierung und modellmäßige Beschreibung* (Berichte aus der Werkstofftechnik, Shaker Verlag, Aachen, 2007)
12. P. Pototzky, *Thermomechanisches Ermüdungsverhalten der Hochtemperaturtitanlegierung IMI834* (Fortschritt-Berichte VDI, Reihe 5, Nr. 565, VDI Verlag, Düsseldorf, 1999)
13. R. Teteruk, *Modellierung der Lebensdauer bei thermomechanischer Ermüdungsbeanspruchung unter Berücksichtigung der relevanten Schädigungs-mechanismen* (Fortschritt-Berichte VDI, Reihe 5, Nr. 653, VDI Verlag, Düsseldorf, 2002)
14. A. Jung, *Einfluß einer Partikelverstärkung auf das Hochtemperaturermüdungsverhalten einer dispersions-gehärteten Aluminiumlegierung* (Fortschritt-Berichte VDI, Reihe 5, Nr. 600, VDI Verlag, Düsseldorf, 2000)
15. Ali El-Chaikh, *Charakterisierung der Schädigungs-mechanismen bei thermomechanischer Ermüdung einer hochfesten Titanaluminid-Legierung*, Doctorate Thesis, to be published in 2018
16. H.-J. Christ, V. Bauer, in: *Creep-Fatigue Interactions – Test Methods and Models, ASTM-STP 1539*, A. Saxena und B. Dogan (Eds..), ASTM International, West Consho-hocken, PA, USA, 178 (2011)
17. G. Masing, Wissenschaftliche Veröffentlichungen aus dem Siemens-Konzern **3**, 119 (1923)
18. H.-J. Christ, *Wechselverformung von Metallen* (Springer Verlag, Berlin, Germany, 1991)
19. H.-J. Christ, V. Bauer, Comput. Mater. Sci. **57**, 59 (2012)
20. P. Pototzky, H.J. Maier, H.-J. Christ, Met. Mat. Trans. A **29A**, 2995 (1998)
21. W.J. Ostergren, J. Test. Evaluation **4**, 327 (1976)
22. W.J. Ostergren, E. Krempf, ASME Paper 78-PVP-63, ASME (1978)
23. S. D. Antolovich, S. Liu, R. Baur, Metall. Trans A **12**, 473 (1981)
24. H.-J. Christ, A. El-Chaikh, B. Wollny, in: *LCF8, Eighth International Conference on Low Cycle Fatigue*, T. Beck, E. Charkaluk (Eds.), DVM, Berlin, 87 (2017)
25. H.-J. Christ, V. Bauer, in: *Proc. of the Hael Mughrabi Honorary Symposium: Plasticity, Failure and Fatigue of Structural Materials – From Macro to Nano,* K.J. Hsia, M. Göken, T. Pollock, P.D. Portella, N.R. Moody (Eds.), TMS, Warrendale, 49 (2008)
26. V. Bauer, H.-J. Christ, in: *Proc. Fifth Intern. Conf. On Low Cycle Fatigue,* P.D. Portella, H. Sehitoglu, K. Hatanaka (Eds.), DVM, Berlin, 207 (2004)
27. H. Riedel, *Fracture at High Temperatures* (Springer Verlag, Berlin, 1987)
28. A. Nitta, K. Kuwabara, Current Japanese Materials Research **3**, 203 (1988)
29. A. Nitta, K. Kuwabara, T. Kitamura, *CRIEPI Report E282015*, Central Research Institute of Electric Power Industry, Tokyo (1983)
30. J. Lemaitre, J.L. Chaboche, *Mechanics of Solid Materials* (Cambridge University Press, Cambridge,1990)
31. F. Petry, H.-J. Christ, H. Mughrabi, in: *Microstructure and Mechanical Properties of Materials*, E. Teckhoff, O. Vöhringer (Eds.), DGM-Informationsgesellschft Verlag, Oberursel, 79 (1993)